International Journal of High-Rise Buildings
December 2019, Vol 8, No 4, 291-302
https://doi.org/10.21022/IJHRB.2019.8.4.291

International Journal of
High-Rise Buildings
www.ctbuh-korea.org/ijhrb/index.php

Optimization Calculations and Machine Learning Aimed at Reduction of Wind Forces Acting on Tall Buildings and Mitigation of Wind Environment

Hideyuki Tanaka[1†], Yasutomo Matsuoka[2], Takuma Kawakami[2], Yasuhiko Azegami[1], Masashi Yamamoto[1], Kazuo Ohtake[1], and Takayuki Sone[1]

[1]Takenaka Corporation, Inzai, Chiba, Japan
[2]Takenaka Corporation, Shinsuna, Koto-ku, Tokyo, Japan

Abstract

We performed calculations combining optimization technologies and Computational Fluid Dynamics (CFD) aimed at reducing wind forces and mitigating wind environments (local strong winds) around buildings. However, the Reynolds Averaged Navier-stokes Simulation (RANS), which seems somewhat inaccurate, needs to be used to create a realistic CFD optimization tool. Therefore, in this study we explored the possibilities of optimizing calculations using RANS. We were able to demonstrate that building configurations advantageous to wind forces could be predicted even with RANS. We also demonstrated that building layouts was more effective than building configurations in mitigating local strong winds around tall buildings. Additionally, we used the Convolutional Neural Network (CNN) as an airflow prediction method alternative to CFD in order to increase the speed of optimization calculations, and validated its prediction accuracy.

Keywords: Optimization calculation, CFD, CNN, Wind force, Wind environment

1. Introduction

In recent years, optimization technologies have been utilized for performance enhancement and rationalization of design services in various fields including the architectural field, in which they have been utilized for multiple purposes such as establishing performance criteria and costs in areas such as structural and landscape design (Nakamura, S., et al. (2017), Fujiwara, K., et al. (2018)). A method that combines airflow analysis and optimization technologies is also needed in the wind engineering field for purposes such as "structural configuration design advantageous under wind forces (Elshaer, A., et al. (2017))" and "planning of countermeasures to mitigate local strong winds around buildings (Du, Y., et al. (2019))." Such a method could be applied to more and more cases in the future.

The airflow analysis method generally used in the wind engineering field is Computational Fluid Dynamics (CFD). The turbulence models used in the airflow analysis of urban areas include LES (Large Eddy Simulation) and Reynolds Averaged Navier-stokes Simulation (RANS), and guidelines for their use have been developed (Architectural Institution of Japan (2017); Tominaga, Y., et al. (2008)). However, for the turbulence model to be combined in the process of optimization calculations that require more than 1,000 cases to calculate the optimum solution, it is not realistic to perform an unsteady calculation using LES because of its large calculation load. Therefore, currently there is no option other than using RANS. RANS is widely used to evaluate local strong winds around buildings, but LES, which enables unsteady calculation and is more accurate, is mainly used to calculate wind forces. However, the large calculation loads of LES require long calculation time, so optimization technologies in this field will only become realistic if it is possible to also use RANS to evaluate wind forces. Thus, this paper first refers to the applicability of RANS to optimization technologies by combining RANS with optimization calculations on the configurations and layouts of buildings that contribute to reduction of wind forces. Furthermore, the optimization calculations for reduction of local strong winds around buildings at pedestrian level were separately performed, and then the features of the optimum solutions were compared.

It is predicted that airflow prediction by artificial intelligence ("AI") through such means as a Convolutional Neural Network (CNN) will be turned to practical use as an airflow analysis method as an alternative CFD in the future (e.g., Guo, X., et al. (2016); Umetani, T. and Bickel, B. (2018)). One of the advantages of CNN is that a wind velocity distribution as shown in Figure 1 can be instantly obtained if the user only has the information about multiple

†Corresponding author: Hideyuki Tanaka
Tel: +81-476-47-1700; Fax: +81-476-47-3050
E-mail: tanaka.hideyuki@takenaka.co.jp

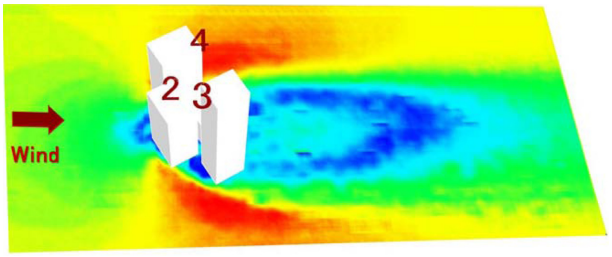


Figure 1. Wind velocity output of tool built on grasshopper.

buildings in the target region as input conditions, compared with CFD which requires wind tunnel tests expertise. This will result in a drastic reduction of calculation time, and will enable a parametric study, short-time optimization calculation and the like. Recent trend has shown that practical researches such as accuracy validation have been in progress in some fields, such as meteorology and the prediction of wind power generation (e.g., Huang, C. J., et al. (2018), Zhou J., et al. (2018) and Harbola S., et al. (2019)). However, no case to the best of our knowledge has validated the predicted accuracy in the field of prediction of airflow around buildings.

Therefore, in this study we assumed an actual urban area, prepared a machine learning model based on the wind velocity distribution around multiple buildings as the learning data and validated its prediction accuracy.

2. Establishment of optimization problem

2.1. Calculation target

The calculation target was assumed to be a 400-by-400-meter development area (Figure 2). The wind that acts on the buildings and the wind velocity in this area were evaluated while making one to four buildings higher and changing their configurations and arrangements. The configurations and layouts of the buildings, as shown in Figure 2, were regarded as the base design (initial values) of the optimization calculations, and the building plan $B = D = 50$ meters and height $H = 200$ meters of these four buildings were considered to be respectively their reference length and reference height.

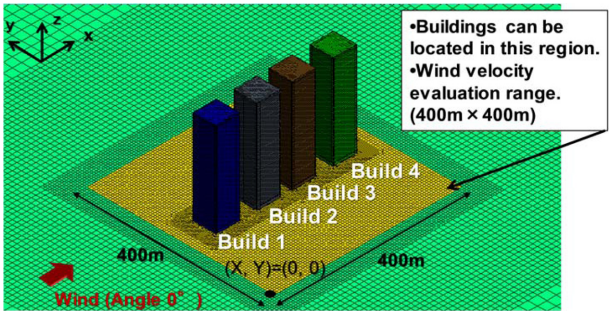


Figure 2. Example of calculation target. (Base design)

2.2. Design variables

The variables of building configuration and location were corner-cut dimensions (b_i, d_i), horizontal rotation angle (θ_i) and central coordinates X_i, Y_i (the corner of the development area shown in Figure 2 was the origin), in addition to building plan dimensions (B_i, D_i) and building height (H_i). Suffix (i) indicates building number (1 to 4). We ensured that we did not to use any extreme building configuration (for instance, a very thin building) for calculation by imposing the constraints listed in Table 1 on these design valuables, such as limiting the gross building volume (V). However, in consideration of design diversity, these conditions were quite loose. Moreover, overlapping two or more buildings was also permitted in laying them out. Adjustments were made so that the gross building volume (V) was constant by adjusting the height of the high-rise section.

2.3. Summary of CFD

We performed CFD analysis for 16 wind directions on the computational domain shown in Figure 3, which included the development area where buildings were laid out with varied configurations and locations, and evaluated the wind forces acting on the buildings and the wind velocity in the development area. The wind forces calculated by the designs were normalized by the mean velocity pressure $q = 60$ Pa, the typical length $B = 50$ m and height $H = 200$ m at $Z_s = 200$ m to get the wind force coefficients C_F, and evaluated as U/U_s, into which the wind velocity

Table 1. Constraint conditions on design valuables

Gross building volume: V	2,000,000 m^3
Building height: H_i	10~500 m
Aspect ratio: $H_i / \sqrt{B_i C_i}$	0.2~10
Ratio of long side to short side: B_i/D_i	0.2~10
Horizontal rotation angle of building: θ_i	0~180 deg.
Corner cutting dimensions at corners of building: b_i (x-direction), d_i (y-direction)	0~0.25 B_i , 0~0.25 D_i
Central coordinates of building: X_i, Y_i	The whole building is contained within the 400-by-400-meter development area.
Distance between buildings: Gap	Overlapping of buildings is permitted, but the high-rise section is adjusted to fix gross building volume (V).

U in the development area was also normalized by the reference wind velocity U_s = 10 m/s.

STAR - CCM + (Ver. 12.02) was used as the analysis code, and steady calculations were performed by using the standard k-ε model, [Note 1)] which was a general RANS model. The inflow boundary conditions shown in Table 2 were defined to get the turbulent boundary layer flow in roughness category III. Other methods and boundary conditions were determined as listed in Table 1, by reviewing the Guidelines (Tominaga, Y., et al. (2008)) for reference. In addition, for calculations in the computational domain, layer meshes were located on the building surfaces, and then meshes for the development area region (Level 2, Figure 4 (b)), for the circular building regions (Level 1, Figure 4 (a)) and for the whole computational domain (Level 0, Figure 4 (a)) were formed out of 2.5m meshes established on the building surfaces (Level 3, Figure 4 (c)), using Levels 0 to 4 trim meshes. The Level-4 mesh size was established to be used if the building corners were corner cuts (Figure 4 (d)).

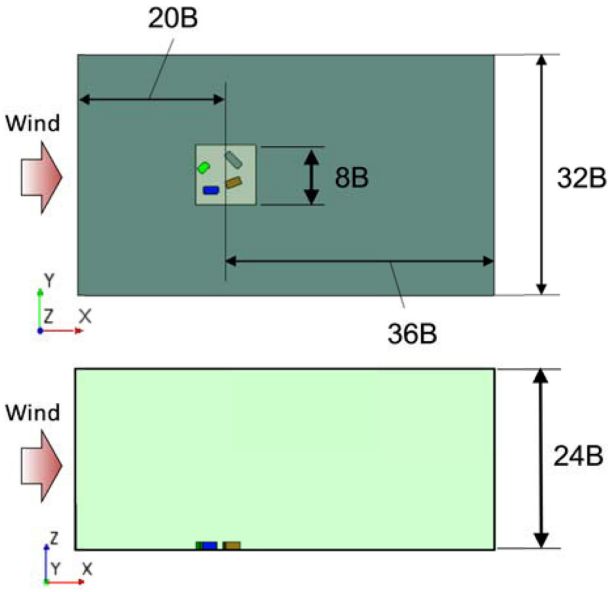


Figure 3. Computational domain of CFD.

Note 1): For the standard k-ε model, the disadvantage of its turbulent energy being overestimated has been also pointed out (e.g., Murakami S., et al. (1990)). Therefore, various modified models such as the LK model (Launder, B. and Kato, M. (1993)) were developed. Especially, the RNG k-ε model (Yakhot, V., et al. (1992)) and the Realizable k-ε model (Shih, T. H., et al. (1995)) represent features of wind flows around buildings relatively well. However, for the wind forces dealt with in this study, it was demonstrated (Miyamoto, K., et al. (1998) and Kawamoto, S., et al. (1998)) that even the modified models could not reproduce the fluctuating wind pressure with sufficient accuracy in the turbulent boundary layer flow. Accordingly, this paper uses the standard k-ε model which is generally used for RANS in comparison with the later-described LES.

2.4. Objective functions

We performed optimization calculations to minimize wind forces and local strong winds around buildings while raising the heights of buildings in the development area. Accordingly, we set H_{max} as an index of maximum building height and maximized it. Simultaneously, $C_{FD,max}$, the maximum along-wind force coefficient of all the buildings for 16 wind directions, was used as an index to evaluate wind forces acting on one to four buildings, and U_{max}/U_s, the maximum wind velocity at 2.0 meters above ground level, which was the maximum for 16 wind directions, was used as an index to evaluate local strong winds around buildings in the development area. In order to compare the features of the optimum solutions, the following calculations were separately performed: One of

Table 2. Calculation method and boundary conditions

Turbulence model	Standard k-ε model, C_μ=0.09
Calculation algorithm	SIMPLE
Convection term scheme	Second-order upwind differencing scheme
Mesh system	Trim meshes (Levels 0-4)
Computational domain	56B(x) × 32B (y) × 24B (z)
Inflow boundary conditions	Wind velocity: $U_{inlet} = U_s\left(\frac{Z}{Z_s}\right)^{\alpha}$, U_s = 10 m/s, Z_s = 200 m, α = 0.2 Turbulent energy: $k_{inlet} = I\,U_{inlet}$, $I = 0.1\left(\frac{Z}{Z_s}\right)^{-\alpha-0.05}$, Z_G = 450 m Turbulence eddy dissipation: $\varepsilon_{inlet} = C_\mu 0.5\,k_{inlet}\left(\frac{U_S}{Z_s}\right)\alpha\left(\frac{Z}{Z_s}\right)^{\alpha-1}$
Outflow boundary	Gradient zero condition
Lateral and upper boundaries	Gradient zero condition
Floor surface and building wall boundaries	Wall function: = $u^+_{trb} = \frac{1}{\kappa} ln\left(\frac{E}{f} y^+\right)$, κ=0.42, E=9.0, f=1.0

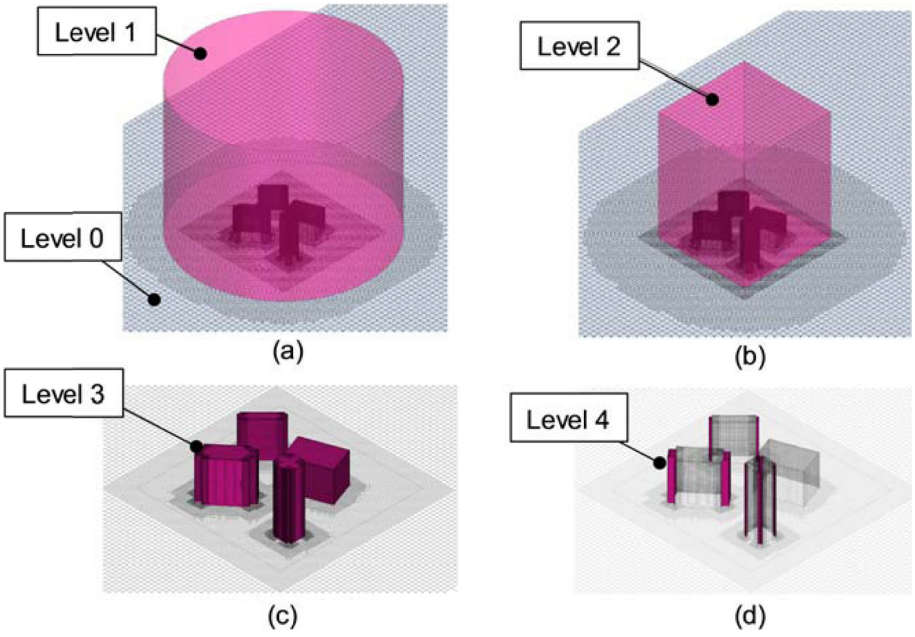


Figure 4. Mesh system. (for calculation of 16 wind directions, Level-1 circular building region rotated every 22.5 degrees.)

them was the calculation with two objective functions, maximization of H_{max} and minimization of the wind force $C_{FD,max}$, and the other was the calculation with the objective functions, maximization of H_{max} and minimization of U_{max}/U_s, the wind velocities of the locally strong winds blowing around buildings. In the optimization calculation of U_{max}/U_s, some restrictions were imposed on the buildings' central coordinates X and Y so that the buildings were not located near the outer perimeter of the evaluation area. This was to prevent the maximum speed U_{max}/U_s from being generated outside the wind velocity evaluation area.

2.4.1. Prediction accuracy of RANS

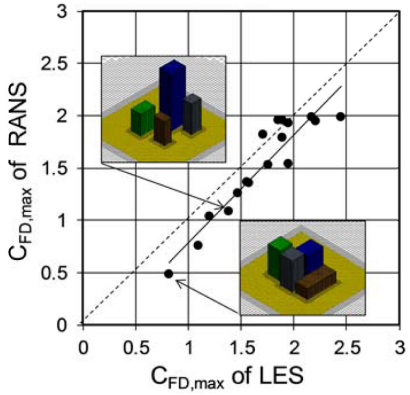
In general, calculation accuracy of wind force coefficient by RANS, which is represented by the standard k-ε model, (a turbulence model), is not as high as that of LES. However, according to the papers written by Miyamoto, et al. (Miyamoto, K., et al. (1998) and Kawamoto, S., et al. (1998)), the calculated mean along-wind force coefficient captures the features relatively well. Therefore, we performed RANS and LES calculations and validated the prediction accuracy of the CFD model shown in 2.3. The numerical wind tunnel Kazamidori, the LES code developed by Takenaka Corporation, was used for accuracy validation. Kazamidori is a tool with highly reliable prediction accuracy, having been often used in wind tunnel tests for accuracy validation (e.g., Tanaka, H., et al. (2013); Tanaka, H., et al. (2014)).

Figure 5 (a) compares the $C_{FD,max}$ results obtained by RANS and LES for wind directions of several building groups. Although the RANS results using the ANS were underestimated compared to the LES results, there were high correlations between them. Hence, we considered it possible to evaluate the wind forces using RANS.

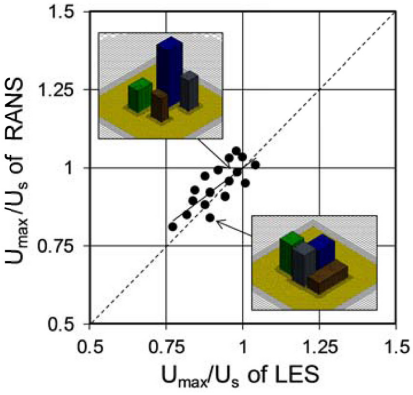
Similarly, Figure 5 (b) compares RANS and LES results for U_{max}/U_s, the maximum wind velocity in the development area. As described in a previous study (Tominaga, Y., et al. (2008)), the prediction accuracy of RANS for the strong wind region, which causes such an issue as local strong winds around buildings, is not low. Their correlations were also high, although the LES results were slightly overestimated. Thus, it is possible to evaluate local strong winds around buildings with maximum wind velocity U_{max}/U_s in the development area.

2.4.2. Validity of objective functions for evaluation of wind forces

Tanaka, Tamura, et al. showed in a previous study (Tanaka, H., et al. (2012)) that the superiority of the aerodynamic characteristics of the various building configurations shown in Figure 6 were highly correlated with the maximum values of the mean wind force coefficients for all directions. The results in Figure 7 show that the maximum along-wind mean force coefficient (maximum mean overturning moments (o.t.m.) $|\overline{C_{MD}}|_{max}$) for all 72 wind directions at equal intervals of 5 degrees are highly correlated with the maximum along-wind fluctuating force coefficients (maximum fluctuating o.t.m. coefficient $C_{MD}'_{,max}$, Figure 7 (a)) for all wind directions and the maximum across-wind mean force coefficients (maximum mean o.t.m. coefficient $|\overline{C_{MD}}|_{max}$, Figure 7 (b)) for all wind directions. These relationships indicate that if the maximum along-wind force coefficient for all directions can be evaluated for multiple target buildings, and their aerodynamic characteristics can be evaluated. Hence, it is also considered in this study that the maximum along-wind

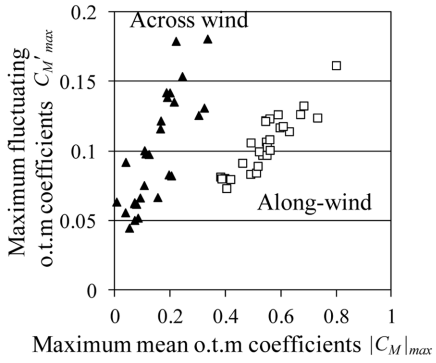


(a) $C_{FD,max}$, Maximum Along-wind Force Coefficients

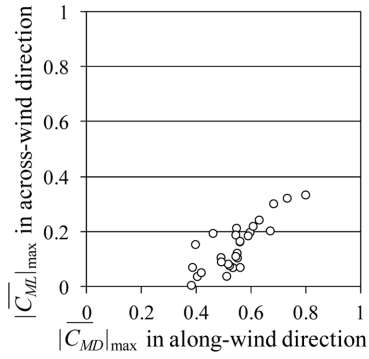


(b) U_{max}/U_s, Maximum Wind Velocities at 2.0 meters above Ground in Development Area

Figure 5. Prediction accuracy validation of RANS compared with LES.



(a) Relationship between Maximum Mean and Maximum Fluctuating O.T.M. Coefficients



(b) Relationship between Maximum Mean O.T.M. Coefficients in Along-wind Direction and in Across-wind Direction

Figure 7. Correlations of maximum along-wind force coefficients in all wind directions. (Tanaka, H., et al. (2012))

force coefficient $C_{FD,max}$ of the four buildings for all directions was calculated according to steady analysis using RANS could be used as an objective function that represents the characteristics of wind forces in optimization calculations.

2.5. Optimization method

Multipurpose optimization with multiple objective

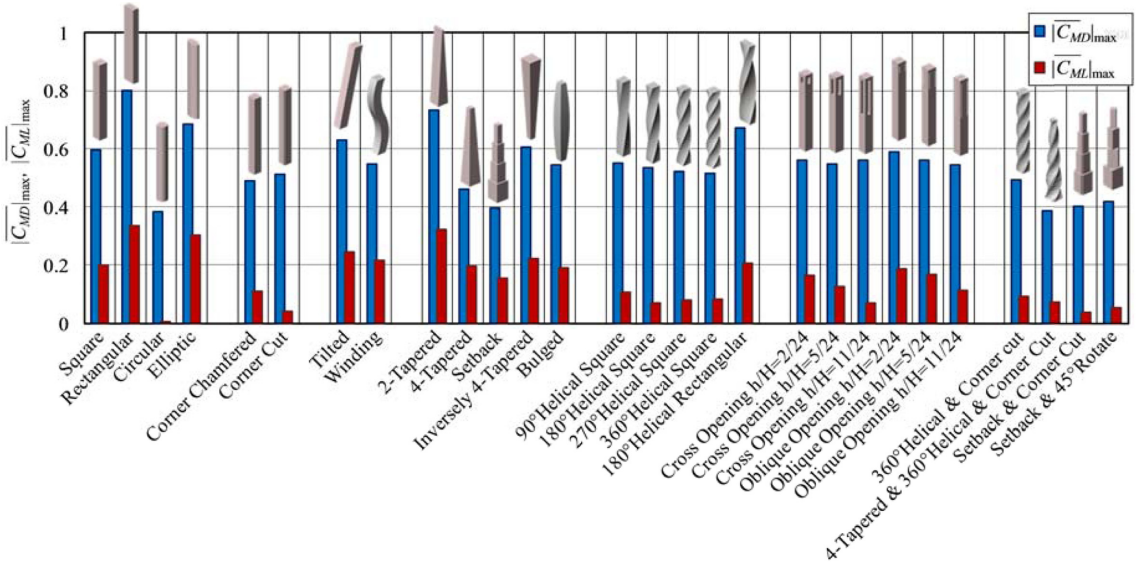


Figure 6. Comparison of maximum mean overturning moment coefficients. (Tanaka, H., et al. (2012))

functions established was performed in this study as discussed earlier. Since a trade-off relationship exists between the objective functions, the optimum solution is not a single solution but is derived as a Pareto front comprising a set of optimum solutions that are on a par with one another. The Systematic Hybrid Exploration is Robust, Progressive, and Adaptive (SHERPA) and is installed on the versatile optimization software HEEDS. It was used for the algorithm for multipurpose optimization to derive this Pareto front. SHERPA is a method of using the Genetic Algorithm (GA), Simulated Annealing (SA), sequential quadratic programming method, etc. separately according to the optimization problem (Red Cedar Technology (2008); Ngo, L. C., et al. (2015)).

3. Results of optimization calculations

3.1. Minimization of wind forces acting on buildings

As a result of optimization calculations with objective functions of maximization of H_{max} and minimization of wind forces $C_{FD,max}$, 675 designs, including five ranking taller than 500 meters, the upper limit of building height, were searched. The evaluated quantity is considered to be enough because it was reported (Red Cedar Technology (2008)) that using the optimization algorithm SHERPA a result close to the optimum value could be acquired even when evaluating and calculating only about 200 cases. Figure 8 shows the Pareto chart of $C_{FD,max}$ and H_{max}. The chart shows the results of all 675 cases calculated, and they are listed in two categories: layout and configuration.

3.1.1. Category I: layout of 4 buildings

Category I-1 is for 4 buildings with square configurations, like the base design in Figure 2. The calculation result for this base design was $C_{FD,max} = 0.76$ at $H_{max} =$ 200 m, ranked No. 139. It can be said as a guide that the smaller the rank No., the closer the building is to the optimum solution. Ranks 55, 607 and 667 are shown as extreme cases of Category I-1 in Figure 8. The three Pareto fronts shown by solid lines in Figure 8 are the estimated set of innumerable optimum solutions in each category. Since both Rank 55 and Rank 667 are on the "Category I" Pareto front, they are a part of the optimum solutions if limited to Category I. These optimum solutions show a tendency in which one or two high-rise buildings with a ratio of long side to short side (B/D) equal to about 1.0 are located. Rank 607, a plate-shaped building with a high B/D, is disadvantageous in terms of wind force characteristics and therefore not an optimum solution. Category I-2, showing a design in which four buildings had corner cuts, was hardly used in this calculation.

3.1.2. Category II: setback

Category II-1 has a setback configuration with multiple square buildings overlapping one another as shown by Ranks 1-3 in Figure 8. The Pareto front of Category II-1 has been improved from that of Category I, with $C_{FD,max}$ reduced at the same building height, which captures the feature of the setback configurations with better wind force characteristics than those of a square building.

Category II-2 has a setback configuration with multiple buildings with corner cuts that overlap one another. In Figure 8, Category II-2 is further categorized into three types according to the categories of corner cut sizes (b, d)

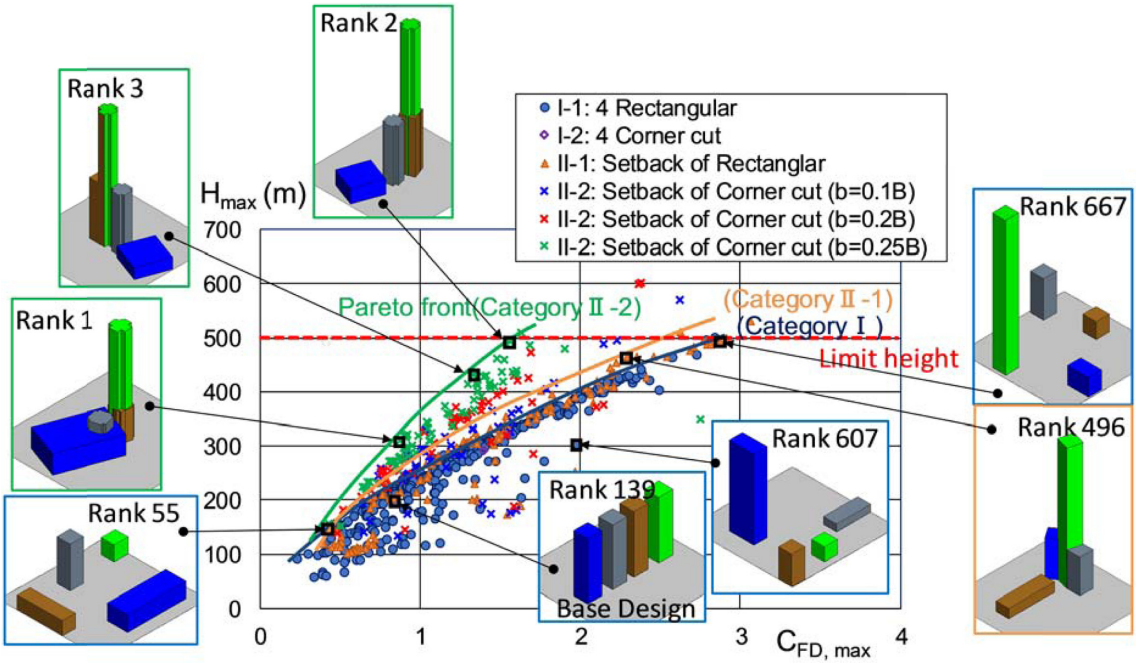


Figure 8. Pareto chart of H_{max} and $C_{FD,max}$.

up to 0.1 B, 0.2 B and 0.25 B. As this corner cut size increases, the $C_{FD,max}$ reduction effect increases. The effect is greater for tall buildings than for low-rise buildings. In particular, the Pareto front of Category II-2 ($b = 0.25$) shown in Figure 8 is greatly improved from those of Categories I and II-1. The feature of the arrangements and configurations of Ranks 1, 2 and 3, which are the optimum solutions in Category II-2, is that one high-rise building with a corner cut size of 0.25 B overlaps multiple buildings, which forms a setback configuration. In particular, the building configurations of Ranks 1 and 2 have setback upper floors rotated approximately 15 degrees with respect to the lower floors on which they are stacked, with many similarities to combined configurations Setback & Corner Cut and Setback & 45° Rotate, which were shown to have good wind force characteristics in a previous study (Tanaka, H., et al. (2012)) (refer to Figure 6).

3.2. Minimization of wind velocity in development area

Figure 9 shows a Pareto chart of calculation results for the 682 cases searched in the optimization calculations with the objective functions of maximization of H_{max} and minimization of U_{max}/U_s, and wind velocities of local strong winds around buildings. In Figure 8 mentioned above, the buildings were categorized mainly by building configuration such as corner cut and setback, by which the Pareto fronts were formed in categories, and consequently we were able to confirm the $C_{FD,max}$ improvement effects according to building configuration. However, Figure 9 shows that the effects are not seen in U_{max}/U_s because the Pareto fronts are not formed by categories.

Under these circumstances, we decided to focus on building layouts rather than building configurations. Although reduction of building volumes and expansion of the development area are expected to improve the degree of freedom of building locations, in this study we changed the gross volume of the buildings set as the fixed conditions to one-eighth, which is equal to 250,000 cubic

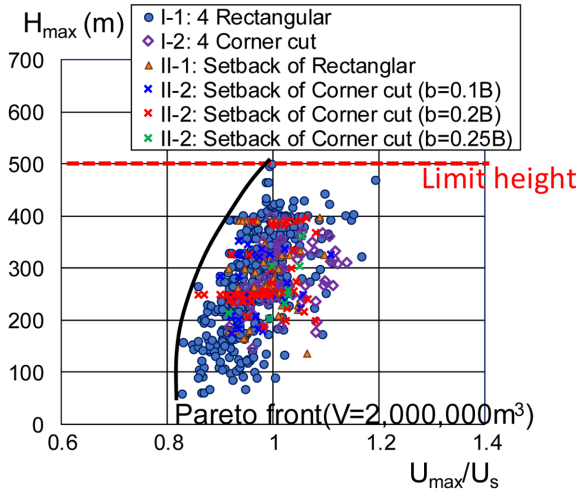


Figure 9. Pareto chart of H_{max} and U_{max}/U_s.

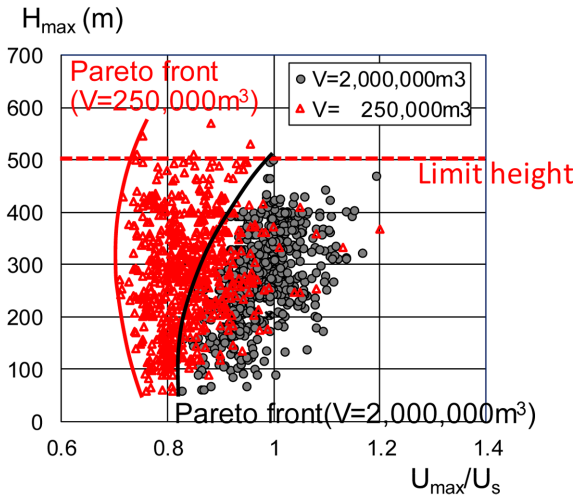


Figure 10. Improvements of pareto front.

meters, and performed similar optimization calculations. Figure 10 shows the optimization calculation results for the 671 designs searched, which are plotted on Figure 9. Figure 10 is a Pareto chart of U_{max}/U_s and H_{max}, where the Pareto front of U_{max}/U_s is greatly improved on the low wind velocity side, which verifies the effect of improving the degree of freedom of the building locations. Thus, the building configuration elements are effective in improving the Pareto fronts in order to minimize the wind forces, while the building arrangements can be said to be more effective than the building configurations for minimizing local strong winds around buildings.

4. Realization of ultrafast prediction of wind environment through machine learning

For CFD by RANS in optimization calculations, 240 parallel computations were performed using the supercomputer (NeXtScale nx360 M5) owned by Takenaka Corporation. Since the computing time was about 3 minutes per wind direction, it took approximately 50 minutes to evaluate one design that required computation for 16 wind directions. Compared with LES, which requires a week's evaluation time, the shorter computation time of CFD by RANS means that it is practical. Yet if the airflow analysis tool for optimization computation can be further sped up, it would make it possible to search for many optimum solutions even for local strong winds around buildings that were hard to evaluate for the building configurations in Section 3.2, which will make cluster analysis, etc. easier and more practical.

The following sections focus on airflow prediction by AI using CNN, which can be expected to increase the speed of airflow analysis more than the CFD, and validate its prediction accuracy.

4.1. Automatic computation of learning data

Although CFD results are used to acquire image data of wind velocity distributions around buildings for machine learning, construction of a high-accuracy machine-learning model requires an enormous amount of image data. Therefore, in this study we automated all the processes using the optimization calculation tool established in Chapter 2, from establishment of a group of buildings for computation, generation of the computational meshes and execution of the solver up to generation of image data, and acquired images for learning data efficiently.

4.2. Computation targets

The layout and configurations of buildings in an actual urban area are varied. However, since this report was aimed at accuracy validation of prediction through CNN, the computation targets for learning data were set for a group of four buildings as shown in Figure 2. The rules for building sizes were also simplified by excluding the horizontal rotational angle (θ), the corner-cut dimensions (b, d) and the building duplications from the constraint conditions on design variables in Table 1. Moreover, as for the optimization calculations for wind velocities, some restrictions were imposed on the range over which the buildings could be located so that the buildings could not be located near the outer perimeter of the evaluation area.

4.3. Construction of machine learning model

4.3.1. Components

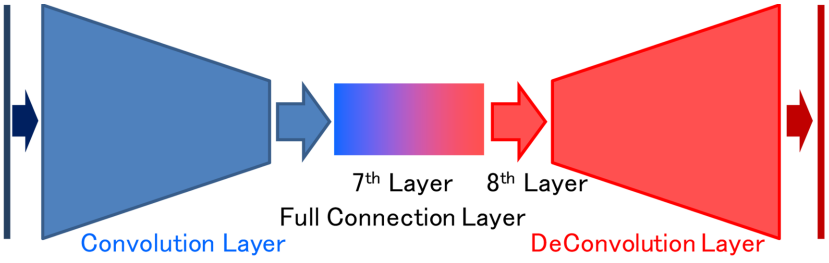
The machine learning model designed in this study consists of the 15 layers of deep learning models shown in Figure 11, which were achieved after comparative experiments with multiple variations. Three types of neural networks were made up of layers: the two-dimensional CNN made up the first to the sixth layers, the Fully connected Neural Network (FNN) made up the seventh and eighth layers and the Deconvolutional Neural Network (DNN) made up the ninth to fifteenth layers. The input image was 316 by 174 pixels, normalized to 0 to 1. The output image was also 316 by 174 pixels, normalized to 0 to 1. For the activation function, all the layers used the Exponential Liner Units (ELU). In the learning, the Mean Squared Error ("MSE") was used for computation of loss values, and the later-described RMSProp for the optimization algorithms. The program is described in Python, and Chainer was used as a deep learning framework.

4.3.2. Comparative experiment on optimization algorithm

Figure 12 shows the results of RMSProp applied as an optimization algorithm and Stochastic Gradient Descent (SGD), which is a basic algorithm, as an example of multiple variations used for comparative experiments. Compared with the teacher data by CFD in Figure 12 (a), SGD has blurred outlines as a whole. However, RMSProp clearly shows the overall state of the wind velocity distribution, from which it can also be confirmed that relative errors is small.

4.3.3. Machine learning model

The machine learning model based on the design in 4.3.1 was created using approximately 3400 pieces of wind velocity distribution image data acquired by automatic CFD calculations as learning and teacher data. Figure 13 shows the learning curve from which it can be confirmed



Layers	CAE FINAL											
	Input			Type	Kernel		Stride		Activation	Output		
1	316	174	1	CNN2D	5	7	1	1	elu	312	168	16
2	312	168	32	CNN2D	2	2	2	2	elu	156	84	32
3	156	84	64	CNN2D	2	2	2	2	elu	78	42	64
4	78	42	128	CNN2D	2	2	2	2	elu	39	21	128
5	39	21	256	CNN2D	13	7	13	7	elu	3	3	512
6	3	3	512	CNN2D	3	3	3	3	elu	1	1	4096
7	4096			Full Connect					elu	2048		
8	2048			Full Connect					elu	2048		
10	1	1	2048	CNN2DT	3	3	3	3	elu	3	3	512
11	3	3	512	CNN2DT	13	7	13	7	elu	39	21	256
12	39	21	256	CNN2DT	2	2	2	2	elu	78	42	128
13	78	42	128	CNN2DT	2	2	2	2	elu	156	168	64
14	156	168	64	CNN2DT	2	2	2	2	elu	312	168	32
15	312	168	32	CNN2DT	5	7	1	1	elu	316	174	1

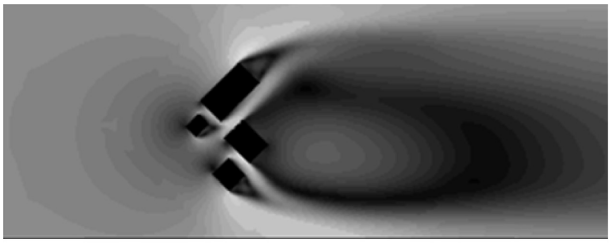
Figure 11. Components of machine learning model.

that learning is advancing while the trend is decreasing. It took about 16 hours to create this model by learning. However, it took only about 0.005 seconds to calculate the test data (the building group information that was not learned), which means that the learning time was reduced to about one-fifty thousandth of that actually spent for CFD, although the computer environments are different.

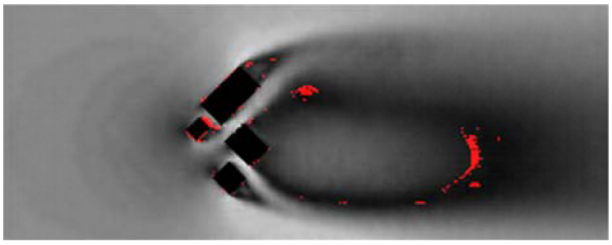
5. Calculation results

5.1. Examples of comparative experiment

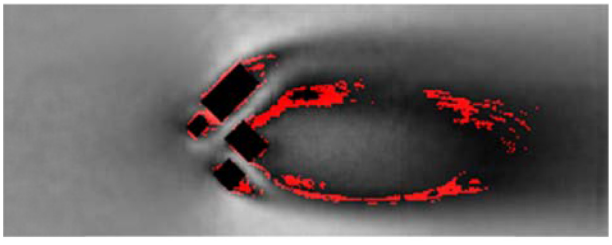
Figure 14 shows some cases of test data calculations. Figure 14 (a) shows a case of buildings arranged in a grid pattern, which is often used in learning data. The relative errors from the CFD results were small in most regions, which resulted in high prediction accuracy. However, Figure 14 (b) shows a case of a different wind direction with the same building group. In this case, the accuracy is not high as indicated by the high relative errors in the wake flow region of the buildings. However, the prediction accuracy is high in the local strong wind region near the corners on the windward side in both cases, which causes the issue of local strong winds around buildings. That is considered to have been caused by a smaller number of similar images, because a pattern for a weak wind region such as a wake flow region is greatly affected by building arrangements and configurations. However, the wind velocity distributions in the strong wind regions had many similarities in the learning images. Furthermore, where the buildings including a plate-shaped building are arranged almost in a line from the two ends of the development area as shown in Figure 15, the prediction accuracy was low because this case was not included in the learning data in this study (Figure 15 (b)).



(a) Teacher data (Correct values, CFD result)



(b) RMSProp



(c) SGD

Figure 12. Differences from optimization algorithm. (The red regions show that the MSREs from the Teacher data are 0.25 or more)

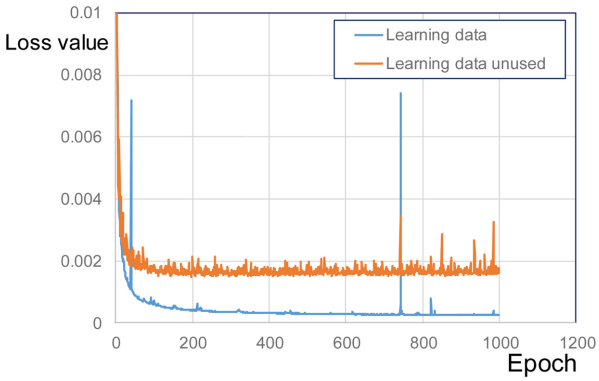


Figure 13. Learning curve of machine learning model.

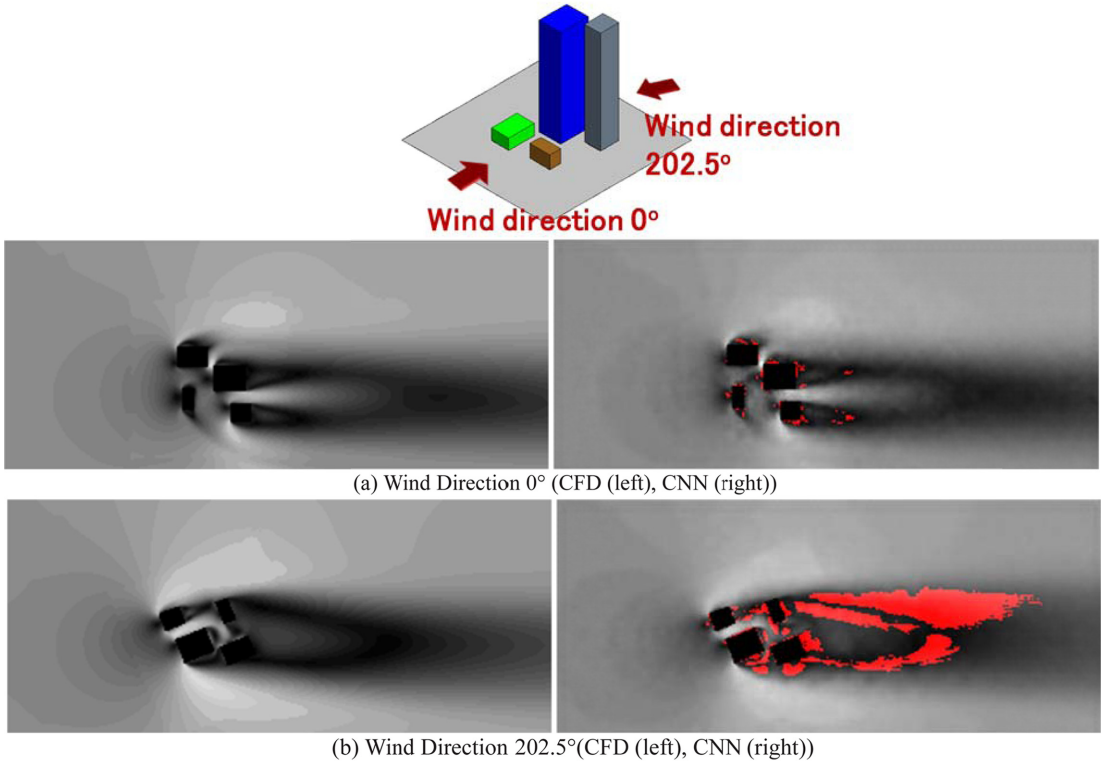
5.2. Improvements by additional learning

Figure 15 (b) shows the results of calculations by image data of wind velocity distributions acquired by performing CFD for which the building layout conditions were relaxed so that the buildings could be located near the outer perimeter of the 400 by 400 meter development area. Figure 15 (c) shows the results of calculations by the additional learning model where approximately 1600 cases were added for learning. Figure 15 (d) shows the results of adding approximately 3800 cases to the learning data to increase the variations of building arrangements. As a result of creating a machine learning model that learned additionally while focusing on the tendency of overfitting, etc. by the learning curve, the prediction accuracy was improved in most of the image data regions depending on the quantities of added learning data.

6. Conclusions

In this study we performed optimization calculations aimed at minimizing wind forces that act with increase in building height and local strong winds around buildings according to building configurations and arrangements by combining optimization technologies with CFD. The following results were obtained:

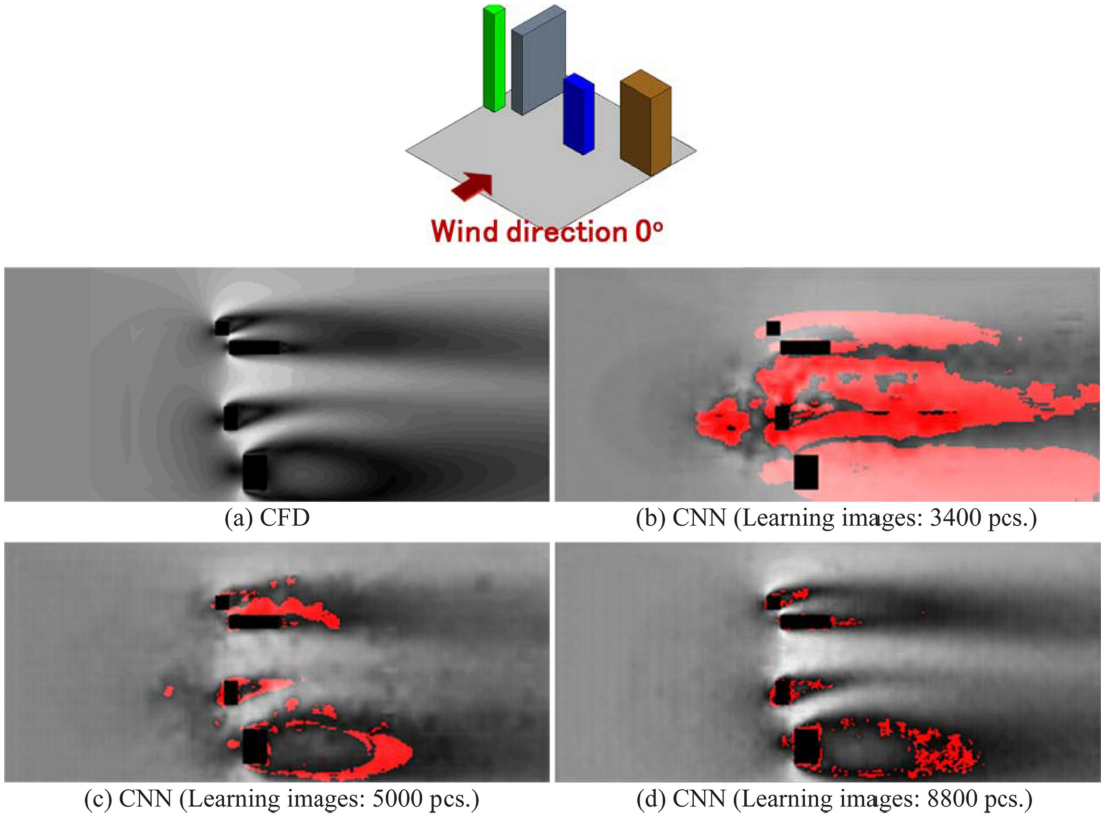
(1) While the prediction accuracy of wind forces by RANS is underestimated compared with LES, comparison of wind forces is possible because of the high correlations. Besides, the prediction accuracy of RANS is also not bad with regard to wind velocities in strong wind regions that



(a) Wind Direction 0° (CFD (left), CNN (right))

(b) Wind Direction 202.5°(CFD (left), CNN (right))

Figure 14. Comparison of prediction accuracies according to wind direction angles. (The red regions show that the relative errors from the CFD are 0.5 or more.)



(a) CFD

(b) CNN (Learning images: 3400 pcs.)

(c) CNN (Learning images: 5000 pcs.)

(d) CNN (Learning images: 8800 pcs.)

Figure 15. Comparison of prediction accuracies according to quantities of learning images. (The red regions show that the relative errors from the CFD are 0.5 or more)

cause issues such as the local strong winds around buildings. Therefore, comparison of maximum wind velocities in the evaluated development area can also be evaluated using RANS.

(2) Steady solutions of maximum along-wind force coefficients for all directions computed by RANS can be used as indices that represent wind force characteristics because they have the high correlation with the aerodynamic characteristics of various building configurations.

(3) As a result of optimization calculations with the objective of maximizing building heights and minimizing wind forces, the highly effective elements were found to be such building configurations as corner cuts and setbacks. Furthermore, the building configurations combining them have greater effects.

(4) As a result of optimization calculations with the objective of maximizing building heights and minimizing wind velocities of local strong winds around buildings, building arrangements are more effective than building configurations.

In order to further speed up the optimization calculations by combining RANS with CFD and making it a practical tool, we have created a machine learning model using CNN, predicted wind flows and validated precision. Results are as follows:

(5) Prediction accuracy of wind velocity distributions in local strong wind regions near corners on the windward side, which is an issue with local strong winds around buildings, is high because of the many similarities even if the amount of learning data is relatively small.

(6) For weak wind regions behind buildings, wind velocity distributions are greatly affected by building arrangements and configurations. Hence, the amount of learning data should be increased to a sufficient quantity to increase the quantity of learning data of similar wind velocity distributions.

(7) Even when the learning data has a small amount of image data of wind velocity distributions for similar building layouts and configurations, we succeeded in improving the prediction accuracy in most regions depending on the quantity of learning data added.

(8) Computation time by CNN to predict wind velocity distributions was reduced to about one-fifty thousandth compared with that by CFD, although the computer environments are different.

References

Architectural Institution of Japan (2017). Guidebook of Recommendations for Loads on Buildings 2 Wind-induced Response and Load Estimation/Practical Guide of CFD for Wind Resistant Design.

Du, Y., Mak, C. M. and Li, Y. (2019). A Multi-stage Optimization of Pedestrian level Wind Environment and Thermal Comfort with lift-up Design in Ideal Urban Canyons, *Sustainable Cities and Society*, 46, 101424.

Elshaer, A., Bitsuamlak, G. and Damatty, A. E. (2017). Enhancing Wind Performance of Tall Buildings using Corner Aerodynamic Optimization, *Engineering Structures*, 136, 133-148.

Fujiwara, K., Asawa, T. and Tsuchiya, N. (2018). Optimization of Tree Arrangement for Landscape Design: Proposal regarding Tree Arrangement Priority Maps for Heat Mitigation, 10th International Conference on Urban Climate in New York, Aug.

Guo, X., Li, W. and Iorio, F. (2016). Convolutional Neural Networks for Steady Flow Approximation, KDD '16, August 13-17, San Francisco, CA, USA.

Harbola S. and Coors V. (2019). One dimensional convolutional neural network architectures for wind prediction, *Energy Conversion and Management*, 195, 70-75.

Huang C. j. and Kuo P. H. (2018). A Short-Term Wind Speed Forecasting Model by Using Artificial Neural Networks with Stochastic Optimization for Renewable Energy Systems, Energies 2018, 11, 2777.

Kawamoto, S., Miyamoto, K., Tsuchiya, N. and Ohtake, K. (1998). Estimation of Wind Loading by Computational Fluid Dynamics Part 2: High-rise Building Case, Summaries of Technical Papers of Annual Meeting 1998 (Transaction of AIJ), pp. 297-298 (in Japanese).

Miyamoto, K., Kawamoto, S. and Tsuchiya, N. (1998). Estimation of Wind Loading by Computational Fluid Dynamics (Part 1) Low-rise Building Case, Summaries of Technical Papers of Annual Meeting 1998 (Transaction of AIJ), pp. 295-296 (in Japanese).

Murakami, S., Mochida, A. and Hayashi, Y. (1990). Examining the k-ε Model by Means of a Wind Tunnel Test and Large-Eddy Simulation of the Turbulence Structure Around a Cube, *Journal of Wind Engineering and Industrial Aerodynamics*, 35, 87-100.

Nakamura, S., Kinoshita, T., Fujii, E., Nakamura, N., Mizushima, Y., Kashima, K, Ikeda, S., Suzuki, T. and Tojo, T. (2017). Section Determination System for Steel Structures Using Decremental Line Search and Automatic member grouping, *J. Struct. Constr. Eng., AIJ*, 82(740), 1609-1619 (in Japanese).

Ngo, L. C., Bello-Ochende, T. and Meyer, J. P. (2015). Three-Dimensional Analysis and Numerical Optimization of Combined Natural Convection and Radiation Heat Loss in Solar Cavity Receiver with Plate Fins Insert, *Energy conversion and management*, 101, 757-766.

Red Cedar Technology (2008). SHERPA - An Efficient and Robust Optimization / Search Algorithm, WP-1023 (Rev. 05.08).

Shih, T. H., Liou, W. W., Shabbir, A., Yang, Z. and Zhu, J. (1995). New k-ε Eddy Viscosity Models for High-Reynolds Number Turbulent Flows, *Computers and Fluids*, 24(3), 227-238.

Tanaka, H., Tamura, Y., Ohtake, K., Nakai, M. and Kim, Y.C. (2012). Experimental Investigation of Aerodynamic Forces and Wind Pressures Acting on Tall Buildings with Various Unconventional Configurations, *Journal of Wind Engineering and Industrial Aerodynamics*, 107-108, 179-191.

Tanaka, H., Tamura, Y., Ohtake, K., Nakai, M., Kim, Y.C. and Bandi, E. K. (2013). Aerodynamic and Flow Characteristics

of Tall Buildings with Various Unconventional Configurations, Int. *Journal of High-Rise Buildings*, 2(3), 213-228.

Tanaka, H., Konno, N., Ohtake, K. and Tsuchiya, N. (2014). Prediction Accuracy of Wind Forces Acting on High-rise Buildings in Urban Areas by Large Eddy Simulation, Proceedings of the 6th International Symposium on Computational Wind Engineering in Hamburg.

Tominaga, Y., Mochida, A, Yoshie, R., Kataoka, H., Nozu, T., Yoshikawa, M. and Shirasawa, T. (2008). AIJ Guidelines for Practical Applications of CFD to Pedestrian Wind Environment around Buildings, *Journal of Wind Engineering and Industrial Aerodynamics*, 96(10-11), 1749-1761.

Umetani, T. and Bickel, B. (2018). Learning Three-Dimensional flow for Interactive aerodynamic design, *ACM Trans. Graph*, 37(4), Article 89.

Yakhot, V., Orszag, S. A., Thangam, S., Gatski, T. B. and Speziale, C. G. (1992). Development of turbulence models for shear flows by a double expansion technique, *Physics of Fluids*, A4, 510-1520.

Zhou J., Liu h., Xu Y. and Jiang W. (2018), A Hybrid Framework for Short Term Multi-Step Wind Speed Forecasting Based on Variational Model Decomposition and Convolutional Neural Network, Energies 2018, 11, 2292.